

Tell Model Where to Look: Mitigating Hallucinations in MLLMs by Vision-Guided Attention

Jianfei Zhao^{1,2}, Feng Zhang¹, Xin Sun^{1,*}, Chong Feng^{1,3,*}, Zhixing Tan^{4,*}

¹School of Computer Science and Technology, Beijing Institute of Technology

²Zhongguancun Academy

³Southeast Academy of Information Technology, Beijing Institute of Technology

⁴Zhongguancun Laboratory

{ zhqingan, bit_zhangfeng, sunxin, fengchong}@bit.edu.cn, zxtan@zgclab.edu.cn

Abstract

Visual attention serves as the primary mechanism through which MLLMs interpret visual information; however, its limited localization capability often leads to hallucinations. We observe that although MLLMs can accurately extract visual semantics from visual tokens, they fail to fully leverage this advantage during subsequent inference. To address this limitation, we propose Vision-Guided Attention (VGA), a training-free method that first constructs precise visual grounding by exploiting the semantic content of visual tokens, and then uses this grounding to guide the model’s focus toward relevant visual regions. In image captioning, VGA further refines this guidance dynamically during generation by suppressing regions that have already been described. In VGA, each token undergoes only a single forward pass, introducing a negligible latency overhead. In addition, VGA is fully compatible with efficient attention implementations such as FlashAttention. Extensive experiments across diverse MLLMs and multiple hallucination benchmarks demonstrate that VGA achieves state-of-the-art dehallucination performance. Further analysis confirms that explicit visual guidance plays a crucial role in enhancing the visual understanding capabilities of MLLMs.¹

1. Introduction

Multimodal Large Language Models (MLLMs) extend the capabilities of large language models (LLMs) into the visual domain, enabling tasks such as visual question answering and image captioning. However, their visual understanding remains limited, as they often exhibit hallucinations—producing outputs that contradict the actual visual

*Corresponding Authors.

¹The code is available at: <https://github.com/beta-nlp/VGA>.

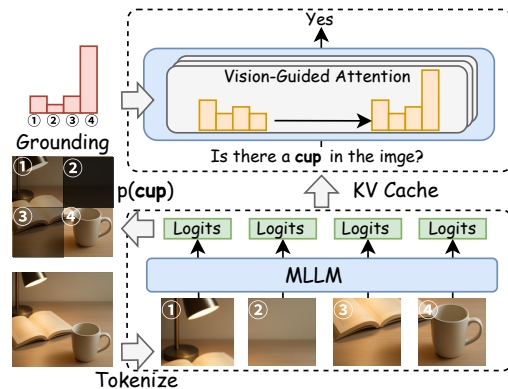


Figure 1. A diagram of vision-guided attention. We first leverage the semantic features embedded in visual tokens to establish visual grounding, and then guide the model’s visual attention toward the relevant image regions.

content. This hallucination issue significantly affects the usability and reliability of MLLMs.

Various approaches have been proposed to mitigate hallucinations, such as constructing targeted datasets [23] or designing specialized loss functions [19, 27]. However, the rapid iteration of model architectures has led to diminishing returns for training-based methods. In contrast, training-free hallucination mitigation techniques offer greater practical value due to their plug-and-play nature and strong generalization capability. In particular, a line of research focuses on optimizing visual attention—a mechanism that serves as the primary conduit through which multimodal large language models (MLLMs) interpret visual information [31, 35]—providing one of the most direct pathways to reducing hallucinations.

Previous studies [18, 28, 30, 37] have underscored the essential role of visual attention in MLLMs and shown that strengthening visual attention can substantially miti-

gate hallucination. However, these approaches depend on the inherent quality of visual attention itself, which is fundamentally limited in its ability to accurately localize critical visual regions [7, 10], ultimately resulting in suboptimal performance. While employing external tools [39] or performing additional forward passes [3] is feasible, these approaches introduce extra computational overhead and reduce practical usability. Furthermore, because they rely on optimization based on attention distributions, they are incompatible with FlashAttention [4], which does not expose explicit attention weights, thereby restricting their applicability. Consequently, optimizing visual attention remains a significant challenge.

To our surprise, we found that the model can accurately extract semantic features from visual tokens and instantiate them as conditional probabilities within the visual logits. This probability distribution over the image enables token-level visual grounding. We term this mechanism Visual Semantic Confidence (VSC). Based on this observation, we propose Vision-Guided Attention (VGA), a novel strategy illustrated in Figure 1 that leverages VSC-derived grounding to identify the most informative visual tokens and direct greater attention toward them. More importantly, VGA does not require computing attention weights for individual tokens, making it fully compatible with FlashAttention.

In short, our main contributions are:

- We introduce Visual Semantic Confidence (VSC), which leverages the semantic features of visual tokens to achieve precise visual grounding.
- We propose Vision-Guided Attention (VGA), a training-free and FlashAttention-compatible method that uses the visual grounding produced by VSC to guide visual attention, enabling the MLLM to focus on the most relevant visual tokens.
- Experiments and analyses demonstrate that VSC provides accurate visual grounding and that VGA effectively mitigates hallucinations in MLLMs.

2. Related Work

Constructing high-quality datasets [2, 23] or designing hallucination-targeted optimization objectives [19, 27] can directly improve model reliability, but the substantial training cost makes these approaches less cost-effective. As a result, training-free dehallucination methods have gained increasing attention. Integrating well-established external tools can effectively enhance the reliability of MLLMs [32, 39], but this also increases the overall system cost. Consequently, optimizing the model’s internal representations has become a more appealing alternative. Such methods mitigate hallucinations by adjusting internal components—such as attention weights, logits, or hidden states—to suppress hallucinatory signals. A line of contrastive decoding-based approaches [11, 14, 33, 38] directly reduces hallucinations

in MLLMs by attenuating hallucinatory features in the logits. However, these methods generally require an additional forward pass to activate or expose such features. Other studies [12, 26, 41] edit semantic features in the embedding space to enhance vision-related representations; yet the high dimensionality and complexity of this space make such vector manipulations prone to introducing noise.

Attention mechanisms serve as the primary means by which MLLMs interpret visual features, and the distribution of attention weights offers an intuitive, interpretable reflection of the model’s visual behavior. Several studies [18, 40] have directly increased the model’s attention to visual content, thereby empirically validating the critical role of visual attention in MLLMs. Other works [6, 29, 36] have investigated functional heterogeneity among attention heads and sought to coordinate their roles accordingly. Additionally, some approaches [10, 30] attribute hallucinations to anomalous attention patterns and propose targeted refinements to address them. While these methods effectively mitigate hallucinations by optimizing visual attention, they largely overlook the inherent variability among visual tokens—specifically, which tokens are most worthy of the model’s attention. Some approaches [28, 37] leverage historical attention distributions to assess the importance of visual tokens and use this information to refine the current attention distribution. However, these methods rely entirely on the model’s inherent visual behavior, which exhibits significant limitations.

Unlike previous works that exploit the limited potential of visual attention itself, we introduce a novel visual prior for visual attention. This prior is derived internally from the model and operates without reliance on external signals. Specifically, we first leverage the semantic features of visual tokens to locate informative ones, and then construct visual guidance based on these locations to modulate the model’s attention.

3. Visual Semantic Confidence

In MLLMs, an input image is first divided into patches, producing visual tokens v_1, \dots, v_m . After encoding by the visual encoder and projector, these visual tokens are concatenated with text embeddings to form a single sequence, which is then fed into the base LLM. The final hidden states are passed through an unembedding matrix to generate logits over the vocabulary. Applying a softmax to the logit at the last position yields the conditional probability for the current generation context, which the model uses to predict the next token: $p(t_i | t_{<i}) \propto \text{softmax}(\text{logit}_{t-1})$.

Logits provide a concrete representation of semantic information [9], where the score associated with each token reflects the model’s confidence in the semantic consistency between that token and the current context. Analogously, visual logits capture the underlying visual semantics of each

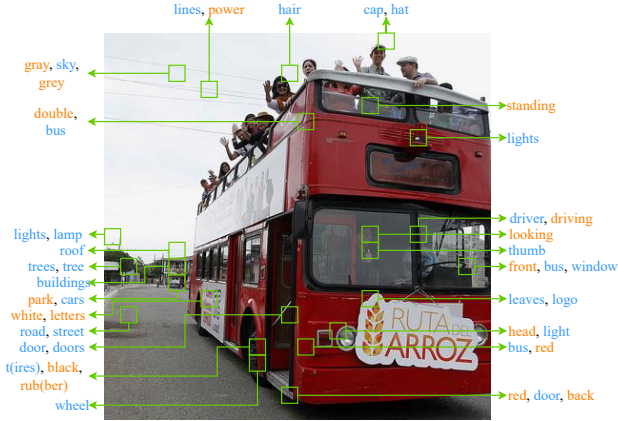


Figure 2. Top-3 tokens (excluding punctuation) in visual logits from LLaVA-1.5-7B.

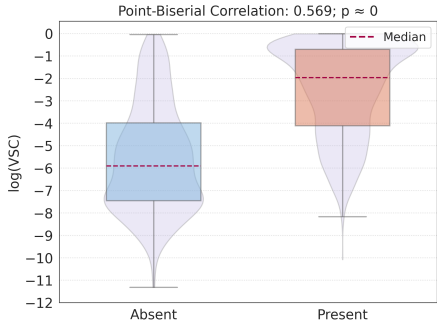


Figure 3. Analysis of visual semantic confidence.

visual token; specifically, the score of a word within the visual logits quantifies the semantic correlation between that word and the corresponding visual context, as illustrated in Figure 2. We term this phenomenon in MLLMs Visual Semantic Confidence (VSC). By aggregating these semantic confidence scores across all visual tokens for a given word, we derive the word’s overall semantic confidence relative to the entire image. Intuitively, **the VSC mechanism can enable token-level visual grounding**. We discuss the VSC mechanism in two scenarios: Section 3.1 details visual grounding with direct visual demands (*e.g.*, VQA), while Section 3.2 addresses cases without explicit visual demands (*e.g.*, image captioning).

3.1. Object-Directed Grounding

The VSC of a visual token v_i with respect to an object O is defined as $c_{v_i}(O) = \text{softmax}[\text{logit}_{v_i}(O)]$. Given the autoregressive nature of MLLMs, we approximate this confidence using the first token o_0 of the tokenized object O (*i.e.*, $c_{v_i}(O) \approx c_{v_i}(o_0)$).

We employ an existence-type VQA task to analyze the relationship between the VSC and the object. We represent

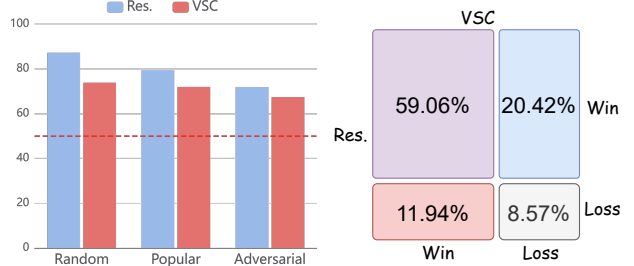


Figure 4. Accuracy comparison of LLaVA-1.5-7B’s response (*Res.*) and its VSC on the POPE benchmark. The threshold of VSC for determining the presence of an object is set to $\log[c(O)] > -2.5$, a value obtained via grid search optimizing the F1 score on the Random subset of the COCO dataset.

the semantic confidence of the entire input image with respect to object O by applying max pooling over all visual tokens:

$$c(O) = \max c_{v_i}(o_0). \quad (1)$$

The analysis results are shown in Figure 3. As observed, VSC exhibits a strong correlation with object presence: objects appearing in the image consistently produce higher semantic confidence scores. This finding indicates that VSC effectively captures the visual semantics encoded in the visual tokens.

VSC serves as an intuitive indicator of an MLLM’s capacity to interpret visual information. We further examine the consistency between VSC and the model’s responses, with results presented in Figure 4. Although object-level judgments derived from VSC are less accurate than the model’s own responses, they still demonstrate a correct preference, significantly exceeding 50% accuracy. In addition, we observe that the understanding reflected by VSC does not always fully align with the model’s responses, revealing a certain degree of preference discrepancy. These findings suggest that an MLLM’s visual understanding is not yet fully exploited, and that the VSC mechanism may be used to enhance the model’s visual perception.

Visual tokens associated with an object exhibit higher VSC values with respect to that object. Leveraging this property, we obtain the visual grounding of the object as:

$$G_O = \text{Norm}[\{c_{v_i}(o_0)\}_{i=1}^m] \in \mathbb{R}^m, \quad (2)$$

where m denotes the number of visual tokens, and $\text{Norm}(\cdot)$ represents sum normalization. To quantify the grounding performance of VSC, we employ the Dice Coefficient [20]:

$$D = \frac{2 \sum_i^m c_i g_i}{\sum_i^m c_i + \sum_i^m g_i}, \quad (3)$$

where $g_i \in [0, 1]$ denotes the overlap coefficient between visual token v_i and the object’s mask annotation. We randomly select 500 images from MSCOCO to evaluate the

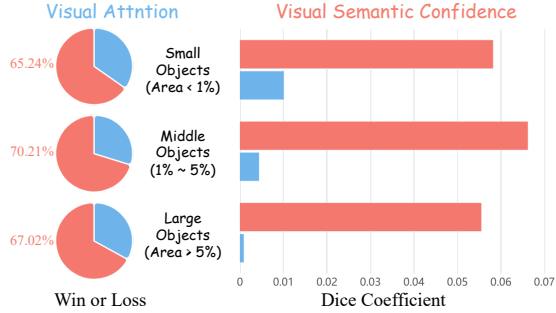


Figure 5. Comparison of visual grounding performance between VSC and the visual attention mechanism of LLaVA-1.5-7B. The visual attention maps are extracted from layer 14, following the prior work [34].

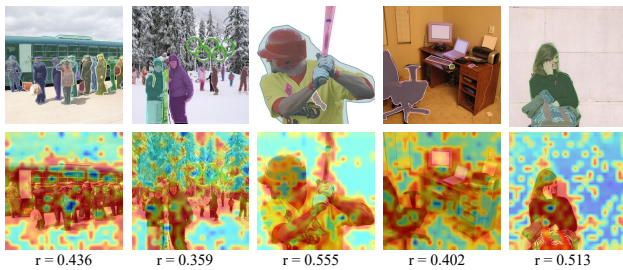


Figure 6. Point-biserial correlation between visual semantic salience and object masks.

grounding capability of VSC and compare it with visual attention. The results are presented in Figure 5. We observe that VSC demonstrates superior grounding capability compared to visual attention. Visual attention suffers from the “sink” phenomenon [10], which limits its grounding ability—particularly for large objects, where it tends to focus only on local regions. In contrast, VSC demonstrates substantially stronger visual grounding performance, exhibiting consistent behavior across objects of different scales. This token-level grounding capability of VSC also provides an indicator of the most informative visual tokens.

3.2. Object-Agnostic Grounding

In VQA tasks, a specific object is often explicitly referenced, enabling the use of VSC for precise object grounding. However, this strategy is not applicable to image captioning, which is inherently object-agnostic. Moreover, in image captioning, the model should not concentrate on a single object; instead, it must attend to all visual information in the image—particularly to visual tokens that encode richer visual content.

We assume that visual tokens rich in visual information should exhibit more definite visual semantics. We employ output uncertainty [37, 41] to measure the semantic salience

in visual tokens:

$$c_{v_i} = - \sum_k \log c_{v_i}(w_k) / \log K, \quad (4)$$

where $\{w_k\}$ are Top- K tokens in logit_{v_i} . To distinguish this approach from VSC, we refer to it as Visual Semantic Saliency (VSS).

The cases in Figure 6 demonstrate the effectiveness of VSS. We observe that tokens corresponding to distinct objects exhibit higher VSS values, whereas semantically insignificant background regions yield lower VSS. Leveraging this property, we construct visual grounding for all objects present in the image.

4. Method

We attribute hallucinations in MLLMs to two primary factors: (1) *Underutilization of extracted visual features*: The model may fail to generate a correct response even when it successfully captures object features with high VSC. (2) *Suboptimal visual attention*: Although visual attention is the main pathway through which the model interprets an input image, it often struggles to accurately focus on the most relevant visual regions. Motivated by these observations, we propose Vision-Guided Attention (VGA), which leverages VSC-derived grounding to direct visual attention toward the most informative tokens.

4.1. Vision-Guided Attention

Due to the autoregressive nature of MLLMs, we can pre-process the visual tokens to compute the VSC and then leverage the caching mechanism to continue generating the response, ensuring that each token undergoes only a single forward pass. We first use NLP tools to extract the objects mentioned in the question and then construct visual grounding through the VSC mechanism. When multiple objects appear in the question, we apply max pooling over the grounding corresponding to all extracted objects:

$$\mathbf{G} = \max_j \mathbf{G}_{O_j} \in \mathbb{R}^m, \quad (5)$$

where \mathbf{G}_{O_j} is defined in Equation (2), and m is the number of visual tokens, satisfying $m = e - s$. We use \mathbf{G} to guide the model’s visual attention:

$$\hat{\alpha}_{h,-1,s:e} = \alpha_{h,-1,s:e} + \beta \cdot \mathbf{G}, \quad (6)$$

where β is a hyperparameter, and $\alpha \in \mathbb{R}^{H \times L \times L}$ denotes the attention weights, with H representing the number of attention heads and L the sequence length. The model then applies the guided attention weights to compute self-attention:

$$\hat{z} = \hat{\alpha} \mathbf{V}, \quad (7)$$

where V denotes the value embeddings, and \hat{z} represents the self-attention output embeddings.

Attention acceleration techniques such as FlashAttention provide high computational efficiency, making them the preferred choice in most MLLM applications. However, these methods do not explicitly output attention weights (*i.e.* α), rendering various attention-based optimization approaches incompatible. In contrast, VGA optimizes attention using visual grounding derived from VSC; since it does not require the computation of attention weights, it remains fully compatible with FlashAttention.

VGA can be optimized using the associative property of addition:

$$\hat{z} = (\alpha + \beta \cdot G)V = z + \beta \cdot \Delta z, \quad (8)$$

where z denotes the output embeddings of vanilla self-attention

4.2. Attention Heads Balancing

The multi-head attention mechanism inherently promotes spontaneous specialization among attention heads, resulting in certain heads naturally developing visual functionalities. To prevent disruption to the model’s intrinsic visual capabilities, we balance the guidance strength across attention heads: weaker guidance is applied to visually specialized heads, while stronger guidance is employed for non-visual heads. The update for the attention mechanism is formulated as follows:

$$\hat{z} = z + \beta \cdot \gamma \cdot \Delta z, \quad (9)$$

where $\gamma \in \mathbb{R}^H$ represents the balancing coefficients across the attention heads. To approximate the discrepancy in visual functionality across all attention heads, we utilize the similarity between z and Δz :

$$\gamma' = \text{Norm}(\text{sim}(z, \Delta z)) \in \mathbb{R}^H, \quad (10)$$

where $\text{Norm}(\cdot)$ is the sum normalization and $\text{sim}(\cdot, \cdot) \in [0, 1]$ is the cosine similarity. A higher similarity value for a particular head signifies a more pronounced visual functionality. Finally, we scale this discrepancy to have a mean of 1 and then invert it to obtain the final balancing coefficient

$$\gamma = \text{ReLU}(2 - H \cdot \gamma'), \quad (11)$$

where H is the number of attention heads.

4.3. Programmed Vision-Guidance

In VQA tasks, visual demands are typically static and remain unchanged throughout the inference process. In contrast, image captioning involves dynamically evolving visual demands as the description is being generated. Consequently, a constant vision grounding mechanism is insufficient to adequately meet the varying visual requirements of image captioning tasks.

To enable visual grounding that dynamically adapts to these changing visual demands during the generation process, we propose the Programmed Visual Grounding (PVG) mechanism. Specifically, during text generation, we dynamically adjust the visual grounding by suppressing regions associated with content that has already been generated.

The adjustment of the visual grounding is performed as follows:

$$G_{t+1} = (1 + \lambda)G_t - \lambda G_w, \quad (12)$$

where w is the token generated at the current step and λ is a hyperparameter controlling the change intensity. This adjustment mechanism effectively shifts the vision grounding of guidance away from regions associated with already generated content G_w and toward regions relevant to the yet-to-be-generated content. Subsequently, the visual grounding is sum-normalized as follows:

$$G'_{t+1} = \text{Norm}(\text{ReLU}(G_{t+1})). \quad (13)$$

In image captioning tasks, as more content is generated, the guidance shifts toward less informative regions via the PVG mechanism, and the model’s dependency on visual information gradually decreases [28]. Accordingly, the vision-guidance should be progressively weakened. The attention update mechanism presented in Equation (9) is therefore modified to incorporate this decay:

$$\hat{z} = z + \|G\|_0 \cdot \gamma \cdot \beta \cdot \Delta z, \quad (14)$$

where $\|G\|_0$ is the L0 norm of G .

5. Experiments

5.1. Experimental Setup

Benchmarks & Baselines. Our method is evaluated on three hallucination benchmarks: POPE [13] (VQA), CHAIR [22] (image captioning), and AMBER [25] (hybrid). We select three recent visual attention-based de-hallucination methods for comparative analysis: PAI [18], VAF [30], TARAC [28]. We denote the variants of PAI with and without contrastive decoding as PAI_{CD} and PAI, respectively.

Implementation Details. Following the established practice of PAI, we determine the starting layer for VGA based on the *BOS* attention. Specifically, the starting layers are set as follows (with layers numbered from 0): layer 2 for LLaVA-1.5, layer 0 for LLaVA-Next, and layer 4 for Qwen2.5-VL. We apply VGA up to an intermediate layer of the model: specifically, layer 24 for LLaVA-1.5-13B and layer 16 for all other models. We adopt the default settings of $\beta = 0.2$ and $\lambda = 0.02$. For the larger model (LLaVA-1.5-13B) and visually simpler tasks (POPE), we increase γ

Table 1. Results on POPE. The results are reported as the average performance across the MSCOCO, A-OKVQA, and GQA datasets. **Bolded** values indicates the best results and underlined values indicates the second-best results. *Acc.* stands for Accuracy.

	Method	LLaVA-7B		LLaVA-13B		LLaVA-Next		Qwen2.5-VL	
		Acc. \uparrow	F1 \uparrow	Acc. \uparrow	F1 \uparrow	Acc. \uparrow	F1 \uparrow	Acc. \uparrow	F1 \uparrow
Random	Vanilla	87.12	87.94	84.31	85.96	87.36	85.90	89.88	89.10
	PAI	86.20	87.20	85.36	86.71	87.71	86.34	<u>90.85</u>	<u>90.31</u>
	PAI _{CD}	<u>87.27</u>	<u>87.98</u>	86.10	87.24	-	-	-	-
	VAF	84.88	86.34	82.42	84.62	<u>89.31</u>	<u>88.45</u>	90.57	89.87
	TARAC	86.99	<u>87.80</u>	<u>87.02</u>	87.80	86.13	84.26	89.79	89.01
	VGA	89.28	89.41	88.58	89.07	89.91	89.21	91.08	90.57
Popular	Vanilla	79.38	82.14	78.64	81.87	85.45	84.14	87.88	87.24
	PAI	78.45	81.56	79.72	82.56	85.95	84.70	<u>87.93</u>	<u>87.65</u>
	PAI _{CD}	<u>80.03</u>	<u>82.51</u>	<u>80.86</u>	<u>83.31</u>	-	-	-	-
	VAF	77.13	80.82	77.10	80.91	<u>86.58</u>	<u>85.95</u>	87.90	87.41
	TARAC	79.37	82.10	79.40	82.10	83.94	82.25	87.88	87.22
	VGA	83.51	84.73	84.15	85.50	86.62	86.24	88.06	87.81
Adversarial	Vanilla	71.85	77.04	71.58	77.23	82.31	81.40	<u>84.82</u>	84.57
	PAI	70.83	76.46	72.38	77.64	82.64	81.82	84.60	<u>84.82</u>
	PAI _{CD}	<u>72.61</u>	<u>77.38</u>	<u>73.44</u>	<u>78.26</u>	-	-	-	-
	VAF	69.59	75.94	70.08	76.41	83.14	<u>83.00</u>	84.80	84.74
	TARAC	71.92	77.03	71.95	77.03	81.04	79.73	84.72	84.47
	VGA	77.02	79.88	77.01	80.28	<u>83.06</u>	83.22	84.86	85.09

Table 2. Results on CHAIR. Ci and Cs represent the CHAIRi and CHAIRs metric, respectively.

Method	LLaVA-7B			LLaVA-13B			LLaVA-Next			Qwen2.5-VL		
	Cs \downarrow	Ci \downarrow	F1 \uparrow	Cs \downarrow	Ci \downarrow	F1 \uparrow	Cs \downarrow	Ci \downarrow	F1 \uparrow	Cs \downarrow	Ci \downarrow	F1 \uparrow
Vanilla	52.2	13.9	76.1	52.6	14.1	76.4	34.2	9.3	72.2	39.2	<u>9.7</u>	<u>75.0</u>
PAI	33.6	9.0	77.1	40.2	10.8	76.9	34.0	8.9	73.7	<u>36.0</u>	10.3	71.9
PAI _{CD}	<u>30.8</u>	8.1	<u>76.3</u>	<u>37.0</u>	<u>9.9</u>	77.3	-	-	-	-	-	-
VAF	52.4	14.6	75.3	49.6	13.6	76.5	32.8	<u>8.8</u>	<u>72.6</u>	38.2	9.8	74.8
TARAC	43.0	11.2	75.1	43.0	11.2	75.1	<u>29.8</u>	8.0	71.5	39.8	9.8	74.6
VGA	29.8	<u>8.2</u>	<u>76.3</u>	30.0	8.2	<u>77.1</u>	28.6	8.0	71.6	35.4	9.4	75.1

to 0.25 to apply stronger vision guidance. Stanza [21] is utilized to extract objects mentioned in the question. We employ greedy decoding for next token prediction and set the maximum generation length to 512.

Detailed experimental setups are provided in the Appendix A.

5.2. Main Results

POPE results are presented in Table 1. Our proposed method, VGA, achieves significant improvements, clearly demonstrating its advantage in mitigating object hallucinations. The results on CHAIR, shown in Table 2, demonstrate that VGA also performs well on the image captioning task, achieving the lowest overall hallucination rate across all evaluated MLLMs while maintaining a comparable F1

score. Table 3 presents the results on AMBER, where VGA achieves the best overall performance, further validating the effectiveness of VGA.

We provide a more comprehensive discussion of the experimental results in the Appendix B.

5.3. Programmed Vision-Guidance for Image Captioning

For the image captioning task, we first construct visual grounding based on VSS. Subsequently, we dynamically adjust this guidance during generation by suppressing already-described visual regions—a process we term programmed vision-guidance. As illustrated in Figure 7, the precise grounding capability enabled by VSC facilitates the accurate editing of vision-guidance. This mechanism

Table 3. Results on AMBER. The AMBER metric is calculated as $(1 - \text{CHAIR} + \text{F1})/2$.

MLLM	Method	CHAIR ↓	Cover ↑	Hal ↓	Cog ↓	Acc. ↑	Prec. ↑	Rec. ↑	F1 ↑	AMBER ↑
LLaVA-7B	Vanilla	7.1	50.7	32.5	3.8	72.1	92.2	63.0	74.8	34.35
	PAI	5.8	48.8	27.5	2.5	70.3	94.4	58.8	72.5	33.85
	PAI _{CD}	<u>5.1</u>	48.4	<u>25.7</u>	<u>2.1</u>	<u>73.7</u>	<u>93.1</u>	<u>65.2</u>	<u>76.7</u>	<u>36.30</u>
	VAF	6.9	50.7	33.0	3.5	68.7	92.6	57.4	70.9	32.50
	TARAC	5.8	<u>49.3</u>	28.5	2.9	72.0	92.8	62.6	74.8	35.00
	VGA	4.5	48.8	21.6	1.9	76.2	<u>93.1</u>	69.3	79.5	38.00
LLaVA-Next	Vanilla	7.8	63.1	46.1	3.9	85.9	86.5	93.4	89.8	41.50
	PAI	<u>7.1</u>	64.2	42.2	<u>3.2</u>	<u>86.4</u>	87.4	93.0	<u>90.1</u>	<u>42.00</u>
	VAF	7.8	<u>63.2</u>	45.4	3.9	86.0	<u>87.7</u>	91.9	89.7	41.45
	TARAC	6.7	60.3	37.5	3.4	85.8	86.3	93.5	89.8	42.05
	VGA	<u>7.1</u>	62.2	<u>41.4</u>	3.1	86.6	88.4	92.0	90.2	42.05
Qwen2.5-VL	Vanilla	4.8	64.8	25.9	1.5	86.5	87.3	93.2	90.1	43.15
	PAI	7.1	60.3	34.7	1.6	86.0	<u>88.1</u>	91.2	89.6	41.75
	VAF	4.7	64.2	<u>25.1</u>	<u>1.4</u>	85.7	<u>87.1</u>	92.1	89.5	42.90
	TARAC	<u>4.8</u>	65.2	26.5	1.5	86.6	87.8	<u>92.7</u>	<u>90.2</u>	43.20
	VGA	4.7	61.8	24.2	1.3	87.1	88.5	92.5	90.5	43.40

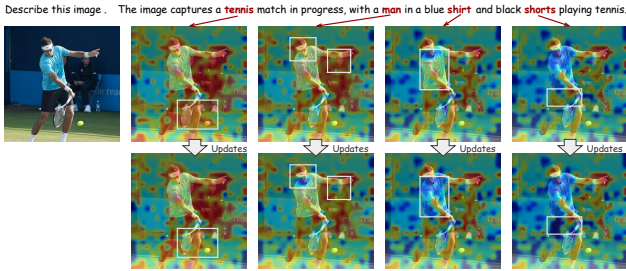


Figure 7. Programmed Vision-Guidance. We set γ to 0.1 in this case to better illustrate the dynamic process.

Table 4. PVG represents Programmed Vision-Guidance. Reversed VSS denotes initial vision guidance by $1 - G$ in Eq. (2).

Setting	Cs	Ci	R	F1
VGA	29.8	8.2	70.4	76.3
Reversed VSS	30.6	8.6	69.5	75.9
w/o PVG	22.2	5.6	65.0	74.5

effectively steers the model to focus more on previously undescribed regions, promoting comprehensive and non-redundant caption generation.

We conduct an ablation study comparing PVG with static VSS-based grounding, with the results presented in Table 4. First, guiding the model to focus on semantically rich regions effectively improves image captioning quality by encouraging the generation of more meaningful and informative content. Conversely, increasing attention to low-

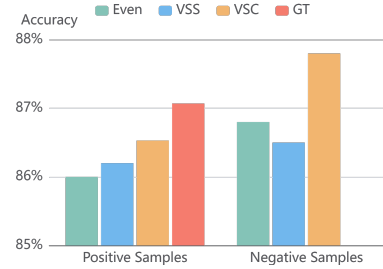


Figure 8. Accuracy on positive and negative samples in POPE with different vision-guidance. *Even* denotes uniform attention allocation across all visual tokens, while *GT* refers to the use of ground-truth grounding.

semantic regions not only leads to a rise in hallucinations but also results in a decline in recall, as the model generates less relevant or redundant descriptions. Moreover, models operating without dynamic adjustment of visual guidance tend to produce more concise descriptions. While this static approach may reduce hallucination rates, it concurrently leads to the omission of important visual details. In summary, PVG significantly enhances MLLM performance in image captioning. It achieves this by balancing detail preservation and hallucination suppression through adaptive visual grounding, thereby mitigating the trade-off inherent in static grounding methods.

5.4. Vision-Guidance Enhancing MLLM’s Visual Perception

VGA employs VSC grounding to guide visual attention, leading to significant performance gains on the POPE

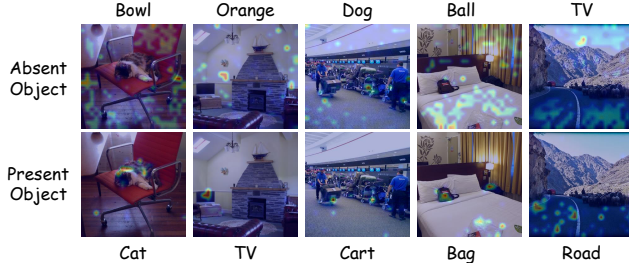


Figure 9. VSC grounding for absent and present objects.

benchmark. To better understand the role of grounding, we further investigate two critical questions: (1) *Why does grounding for absent objects still effectively improve the model’s object perception?* (2) *What will happen when VSC grounding is unreliable?*

5.4.1. Analysis of Negative Samples

Figure 8 illustrates the effects of different visual grounding strategies on both positive and negative samples. First, in positive samples—where the queried object is present—the model’s object perception consistently improves as the visual grounding becomes more precise. This demonstrates that providing precise visual grounding effectively enhances MLLM’s overall visual understanding. Moreover, in negative samples—queries about objects absent from the image—the application of VSC still significantly improves the model’s ability to correctly reject the presence of such objects.

Figure 9 presents the VSC-based grounding maps for both present and absent objects. We find that VSC enhances the model’s perception for absent objects by redirecting attention toward low-semantic regions (*i.e.*, background or uninformative areas), allowing the model to easily infer the object’s absence. In contrast, when guided by VSS-based grounding—which directs attention toward visually richer regions—the model is more prone to misinterpretation, leading to hallucinatory responses.

To quantitatively analyze VSC grounding of negative samples, we define high-semantic regions (above-mean) based on the VSS distribution. We introduce the Informative Coefficient (IC), defined as the sum of VSC weights (sum-normalized) over these high-semantic regions. The average IC is 0.64 for positive samples and 0.42 for negative samples, indicating that visual guidance in negative samples concentrates on low-semantic regions. Moreover, false positives (FPs) exhibit an average IC of 0.57, whereas true negatives (TNs) show an average of 0.41. After randomly sampling TNs to match the FP count, we analyze their correlation; the average Pearson correlation between IC and FP is $r = 0.414 \pm 0.019$. These results demonstrate that VSC effectively shifts attention away from high-semantic regions in negative contexts, thereby reducing FPs.

5.4.2. Spurious VSC Grounding

We analyze the performance of VGA under conditions of imprecise visual grounding. On positive samples, VGA employing spurious VSC grounding with a low Dice Coefficient ($DICE < 0.01$) achieves an accuracy of 88.5%, compared to 87.1% for VGA with uniform guidance. We attribute the beneficial effect of spurious grounding to information flow: final visual hidden states inherently incorporate features from preceding visual tokens, resulting in a misalignment between vision grounding and feature grounding. Therefore, although VSC localization may be visually suboptimal in some cases, it still provides correct positional preferences.

We further analyze the failure cases of VGA. We observe that true positives exhibit significantly higher average DICE scores (0.0475) compared to false negatives (0.0006). In these failure cases, the visual grounding constructed by VSC exhibits extremely low precision. This is attributed to the model’s inability to effectively extract visual features, which renders the VSC derived from degraded visual logits ineffective. In the absence of external cues, failures in visual feature extraction inevitably lead to erroneous understanding. Nevertheless, the consistent performance improvements across various baselines indicate that the VSC mechanism possesses robust visual localization capabilities.

In short, precise vision guidance is crucial for the model’s visual understanding, and the VSC mechanism provides reliable guidance.

5.5. The Evaluation of Latency

Both the construction of VSC grounding and the update of vision guidance via PVG utilize pre-computed visual logits (fixed during inference), requiring no additional forward passes. We evaluate Time to First Token (TTFT) using LLaVA-1.5-7B on the AMBER benchmark, where VGA incurs only a 4.36% increase. Additionally, we evaluate Time Per Output Token (TPOT) on CHAIR, where VGA introduces a 6.01% overhead. In short, our method is well-compatible with the model’s autoregressive nature, incurring only minimal latency overhead.

6. Conclusion

In this work, we propose a Visual Semantic Confidence mechanism to construct accurate visual grounding without relying on external tools. Building upon this, we introduce Vision-Guided Attention, a novel mechanism that leverages the derived visual grounding to steer the model’s visual attention toward the most informative regions, thereby effectively mitigating hallucinations in MLLMs. Moreover, it requires only a single forward pass per token, incurs negligible additional inference cost, and is compatible with FlashAttention.

Acknowledgments

We thank all reviewers for their detailed reviews and valuable comments. This work is supported by Zhongguancun Academy Project No.20240103.

References

- [1] Shuai Bai, Keqin Chen, Xuejing Liu, Jialin Wang, Wenbin Ge, Sibao Song, Kai Dang, Peng Wang, Shijie Wang, Jun Tang, et al. Qwen2.5-vl technical report. *arXiv preprint arXiv:2502.13923*, 2025. 1
- [2] Cong Chen, Mingyu Liu, Chenchen Jing, Yizhou Zhou, Fengyun Rao, Hao Chen, Bo Zhang, and Chunhua Shen. Perturbollava: Reducing multimodal hallucinations with perturbative visual training. In *ICLR*, 2025. 2
- [3] Shiqi Chen, Tongyao Zhu, Ruochen Zhou, Jinghan Zhang, Siyang Gao, Juan Carlos Niebles, Mor Geva, Junxian He, Jiajun Wu, and Manling Li. Why is spatial reasoning hard for vlms? an attention mechanism perspective on focus areas. In *ICML*, 2025. 2
- [4] Tri Dao, Dan Fu, Stefano Ermon, Atri Rudra, and Christopher Ré. Flashattention: Fast and memory-efficient exact attention with io-awareness. In *NeurIPS*, pages 16344–16359, 2022. 2
- [5] Chaoyou Fu, Peixian Chen, Yunhang Shen, Yulei Qin, Mengdan Zhang, Xu Lin, Jinrui Yang, Xiawu Zheng, Ke Li, Xing Sun, Yunsheng Wu, and Rongrong Ji. Mme: A comprehensive evaluation benchmark for multimodal large language models. *arXiv preprint arXiv:2306.13394*, 2024. 4
- [6] Jinghan He, Kuan Zhu, Haiyun Guo, Junfeng Fang, Zhenglin Hua, Yuheng Jia, Ming Tang, Tat-Seng Chua, and Jinqiao Wang. Cracking the code of hallucination in vlms with vision-aware head divergence. In *ACL*, 2025. 2
- [7] Qidong Huang, Xiaoyi Dong, Pan Zhang, Bin Wang, Conghui He, Jiaqi Wang, Dahua Lin, Weiming Zhang, and Nenghai Yu. Opera: Alleviating hallucination in multimodal large language models via over-trust penalty and retrospection-allocation. In *CVPR*, pages 13418–13427, 2024. 2
- [8] Drew A Hudson and Christopher D Manning. Gqa: A new dataset for real-world visual reasoning and compositional question answering. In *CVPR*, pages 6700–6709, 2019. 1
- [9] Nicholas Jiang, Anish Kachinthaya, Suzanne Petryk, and Yossi Gandelsman. Interpreting and editing vision-language representations to mitigate hallucinations. In *ICLR*, 2025. 2
- [10] Seil Kang, Jinyeong Kim, Junhyeok Kim, and Seong Jae Hwang. See what you are told: Visual attention sink in large multimodal models. In *ICLR*, 2025. 2, 4, 3
- [11] Sicong Leng, Hang Zhang, Guanzheng Chen, Xin Li, Shijian Lu, Chunyan Miao, and Lidong Bing. Mitigating object hallucinations in large vision-language models through visual contrastive decoding. In *CVPR*, pages 13872–13882, 2024. 2
- [12] Li Li, Jiashu Qu, Linxin Song, Yuxiao Zhou, Yuehan Qin, Tiankai Yang, and Yue Zhao. Treble counterfactual vlms: A causal approach to hallucination. In *Findings of EMNLP*, pages 18423–18434, 2025. 2
- [13] Yifan Li, Yifan Du, Kun Zhou, Jinpeng Wang, Wayne Xin Zhao, and Ji-Rong Wen. Evaluating object hallucination in large vision-language models. In *EMNLP*, pages 292–305, 2023. 5, 1
- [14] Zhuowei Li, Haizhou Shi, Yunhe Gao, Di Liu, Zhenting Wang, Yuxiao Chen, Ting Liu, Long Zhao, Hao Wang, and Dimitris N Metaxas. The hidden life of tokens: Reducing hallucination of large vision-language models via visual information steering. In *ICML*, 2025. 2
- [15] Tsung-Yi Lin, Michael Maire, Serge Belongie, James Hays, Pietro Perona, Deva Ramanan, Piotr Dollár, and C Lawrence Zitnick. Microsoft coco: Common objects in context. In *ECCV*, pages 740–755, 2014. 1
- [16] Haotian Liu, Chunyuan Li, Yuheng Li, and Yong Jae Lee. Improved baselines with visual instruction tuning. In *CVPR*, pages 26296–26306, 2024. 1
- [17] Haotian Liu, Chunyuan Li, Yuheng Li, Bo Li, Yuanhan Zhang, Sheng Shen, and Yong Jae Lee. Llava-next: Improved reasoning, ocr, and world knowledge, 2024. 1
- [18] Shi Liu, Kecheng Zheng, and Wei Chen. Paying more attention to image: A training-free method for alleviating hallucination in vlms. In *ECCV*, pages 125–140, 2024. 1, 2, 5, 3
- [19] Wenqi Liu, Xueming Song, Jiayi Li, Yinwei Wei, Na Zheng, Jianhua Yin, and Liqiang Nie. Mitigating hallucination through theory-consistent symmetric multimodal preference optimization. In *NeurIPS*, 2025. 1, 2
- [20] Woohyeon Park, Woojin Kim, Jaeik Kim, and Jaeyoung Do. Second: Mitigating perceptual hallucination in vision-language models via selective and contrastive decoding. In *ICML*, 2025. 3
- [21] Peng Qi, Yuhao Zhang, Yuhui Zhang, Jason Bolton, and Christopher D Manning. Stanza: A python natural language processing toolkit for many human languages. In *ACL*, pages 101–108, 2020. 6, 2
- [22] Anna Rohrbach, Lisa Anne Hendricks, Kaylee Burns, Trevor Darrell, and Kate Saenko. Object hallucination in image captioning. In *EMNLP*, pages 4035–4045, 2018. 5, 1
- [23] Pritam Sarkar, Sayna Ebrahimi, Ali Etamad, Ahmad Beirami, Serkan O Arik, and Tomas Pfister. Mitigating object hallucination in mllms via data-augmented phrase-level alignment. In *ICLR*, 2025. 1, 2
- [24] Dustin Schwenk, Apoorv Khandelwal, Christopher Clark, Kenneth Marino, and Roozbeh Mottaghi. A-okvqa: A benchmark for visual question answering using world knowledge. In *ECCV*, pages 146–162, 2022. 1
- [25] Junyang Wang, Yuhang Wang, Guohai Xu, Jing Zhang, Yukai Gu, Haitao Jia, Jiaqi Wang, Haiyang Xu, Ming Yan, Ji Zhang, et al. Amber: An llm-free multi-dimensional benchmark for mllms hallucination evaluation. *arXiv preprint arXiv:2311.07397*, 2023. 5, 1
- [26] Kaishen Wang, Hengrui Gu, Meijun Gao, and Kaixiong Zhou. Damo: Decoding by accumulating activations momentum for mitigating hallucinations in vision-language models. In *ICLR*, 2025. 2
- [27] Wenyi Xiao, Ziwei Huang, Leilei Gan, Wangui He, Haoyuan Li, Zhelun Yu, Fangxun Shu, Hao Jiang, and Lin-

- chao Zhu. Detecting and mitigating hallucination in large vision language models via fine-grained ai feedback. In *AAAI*, pages 25543–25551, 2025. 1, 2
- [28] Chunzhao Xie, Tongxuan Liu, Lei Jiang, Yuting Zeng, Yunheng Shen, Weizhe Huang, Jing Li, Xiaohua Xu, et al. Tarac: Mitigating hallucination in vlms via temporal attention real-time accumulative connection. *arXiv preprint arXiv:2504.04099*, 2025. 1, 2, 5
- [29] Tianyun Yang, Ziniu Li, Juan Cao, and Chang Xu. Understanding and mitigating hallucination in large vision-language models via modular attribution and intervention. In *ICLR*, 2025. 2
- [30] Hao Yin, Guangzong Si, and Zilei Wang. ClearSight: visual signal enhancement for object hallucination mitigation in multimodal large language models. In *CVPR*, pages 14625–14634, 2025. 1, 2, 5
- [31] Hao Yin, Guangzong Si, and Zilei Wang. Lifting the veil on visual information flow in mllms: Unlocking pathways to faster inference. In *CVPR*, pages 9382–9391, 2025. 1
- [32] Shukang Yin, Chaoyou Fu, Sirui Zhao, Tong Xu, Hao Wang, Dianbo Sui, Yunhang Shen, Ke Li, Xing Sun, and Enhong Chen. Woodpecker: Hallucination correction for multimodal large language models. *Science China Information Sciences*, 67(12):220105, 2024. 2
- [33] Ce Zhang, Zifu Wan, Zhehan Kan, Martin Q Ma, Simon Stepputtis, Deva Ramanan, Russ Salakhutdinov, Louis-Philippe Morency, Katia Sycara, and Yaqi Xie. Self-correcting decoding with generative feedback for mitigating hallucinations in large vision-language models. In *ICLR*, 2025. 2
- [34] Jiarui Zhang, Mahyar Khayatkhoei, Prateek Chhikara, and Filip Ilievski. Mllms know where to look: Training-free perception of small visual details with multimodal llms. In *ICLR*, 2025. 4
- [35] Zhi Zhang, Srishti Yadav, Fengze Han, and Ekaterina Shutova. Cross-modal information flow in multimodal large language models. In *CVPR*, pages 19781–19791, 2025. 1
- [36] Jianfei Zhao, Feng Zhang, Xin Sun, and Chong Feng. Mitigating hallucination in large vision-language models through aligning attention distribution to information flow. In *Findings of EMNLP*, pages 24849–24863, 2025. 2, 3
- [37] Jianfei Zhao, Feng Zhang, Xin Sun, Chong Feng, and Zhixing Tan. Cross-layer vision smoothing: Enhancing visual understanding via sustained focus on key objects in large vision-language models. *arXiv preprint arXiv:2509.12897*, 2025. 1, 2, 4
- [38] Jianfei Zhao, Feng Zhang, Xin Sun, Lingxing Kong, Zhixing Tan, and Chong Feng. Cross-image contrastive decoding: Precise, lossless suppression of language priors in large vision-language models. *arXiv preprint arXiv:2505.10634*, 2025. 2
- [39] Linxi Zhao, Yihe Deng, Weitong Zhang, and Quanquan Gu. Mitigating object hallucination in large vision-language models via image-grounded guidance. In *ICML*, 2025. 2
- [40] Lanyun Zhu, Deyi Ji, Tianrun Chen, Peng Xu, Jieping Ye, and Jun Liu. Ibd: Alleviating hallucinations in large vision-language models via image-biased decoding. In *CVPR*, pages 1624–1633, 2025. 2
- [41] Xin Zou, Yizhou Wang, Yibo Yan, Yuanhuiyi Lyu, Kenning Zheng, Sirui Huang, Junkai Chen, Peijie Jiang, Jia Liu, Chang Tang, et al. Look twice before you answer: Memory-space visual retracing for hallucination mitigation in multimodal large language models. In *ICML*, 2025. 2, 4

Tell Model Where to Look: Mitigating Hallucinations in MLLMs by Vision-Guided Attention

Supplementary Material

A. Detailed Experimental Setup

Evaluated MLLMs. We evaluate the effectiveness of our proposed method, Vision-Guided Attention (VGA), on three representative MLLMs: **LLaVA-1.5** [16], **LLaVA-Next** [17], and **Qwen2.5-VL** [1]. LLaVA-1.5 is available in two sizes: 7B and 13B. Both LLaVA-Next and Qwen2.5-VL are 8B-scale

A.1. Benchmarks

In order to validate the effectiveness of our method in mitigating hallucination, we evaluate its performance on three widely-used multimodal hallucination benchmarks: one generative benchmark (CHAIR [22]), one discriminative benchmark (POPE [13]), and one hybrid benchmark (AMBER [25]).

CHAIR. CHAIR evaluates the proportion of hallucinated objects, which are generated by the model but not present in the reference annotations. Following prior works, we randomly select 500 images from the MSCOCO [15] dataset as the test set. We additionally select another 500 images to construct a validation set for hyperparameter tuning. This benchmark includes two metrics: CHAIRs and CHAIRi, defined as follows:

$$\begin{aligned} \text{CHAIRs} &= \frac{|\text{Hallucinated Objects}|}{|\text{All Objects}|}, \\ \text{CHAIRi} &= \frac{|\text{Hallucinated Captions}|}{|\text{All Captions}|} \end{aligned} \quad (16)$$

POPE. POPE is a widely adopted benchmark for evaluating object hallucinations by prompting LVLMS to identify whether a specific object is present in the image. It comprises three distinct datasets: *MSCOCO* [15], *AOKVQA* [24], and *GQA* [8]. Each dataset uses three different negative sampling settings: *Random*, *Popular*, and *Adversarial*. Each subset includes 3,000 questions and 500 images. Accuracy and F1 score are used as the primary evaluation metrics.

AMBER. AMBER combines generative and discriminative tasks, and is evaluated on a curated set of 1,004 images. In addition to image captioning, it includes 14,216 questions designed to assess hallucinations in object, attribute, and relation recognition. AMBER contains multiple metrics: *CHAIR*, *Cover*, *Hal*, *Cog*. It provides an annotated

objects list $A_{obj} = obj_1^A, obj_2^A, \dots, obj_n^A$, and the generated objects are labeled as R'_{obj} . Each metric is calculated as follows:

$$\begin{aligned} \text{CHAIR} &= 1 - \frac{\text{len}(R'_{obj} \cap A_{obj})}{\text{len}(R'_{obj})}, \\ \text{Cover} &= \frac{\text{len}(R'_{obj} \cap A_{obj})}{\text{len}(A_{obj})}, \\ \text{Hal} &= \frac{\{\text{CHAIR} > 0\}}{\{\text{All Caps}\}}, \\ \text{Cog} &= \frac{\text{len}(R'_{obj} \cap H_{obj})}{\text{len}(R'_{obj})}, \end{aligned} \quad (17)$$

where H_{obj} denotes the set of hallucinated target objects generated by the LVLMS, and *All Caps* refers to all generated captions.

A.2. Baselines

We select three existing visual attention-based dehallucination methods for comparative analysis:²

- **PAI** [18]: This method directly amplifies the model’s attention weights on visual tokens and further enhances visual features using contrastive decoding. To facilitate a fair comparison of visual attention optimization, we denote the variants with and without contrastive decoding as PAI_{CD} and PAI , respectively. We set the visual attention augmentation coefficient α to 0.5 and apply visual attention augmentation starting from the layer specified by our method. PAI_{CD} has a hyperparameter $\gamma = 1.1$ and employs adaptive plausibility constraints with $\beta = 0.1$.
- **VAF** [30]: Similar to PAI , VAF directly scales up visual attention; however, it also suppresses attention on instruction tokens. We set $\beta = 0.1$, $\alpha = 0.15$, and activate this method from layer 9 to layer 14 (counting from 0).
- **TARAC** [28]: This method quantifies the importance of visual tokens based on attention distributions from previous generation steps and utilizes this information to strengthen the model’s focus on relevant visual tokens at the current step. We set $\beta = 0.5$, $\alpha = 0.5$, and activate this method from layer 9 to layer 15 (counting from 0).

A.3. Implementation Details

Following the established practice of PAI , we determine the starting layer for VGA based on the *BOS* attention, which

²Note: The same parameters may have different meanings across methods. For specific details, please refer to the original papers.

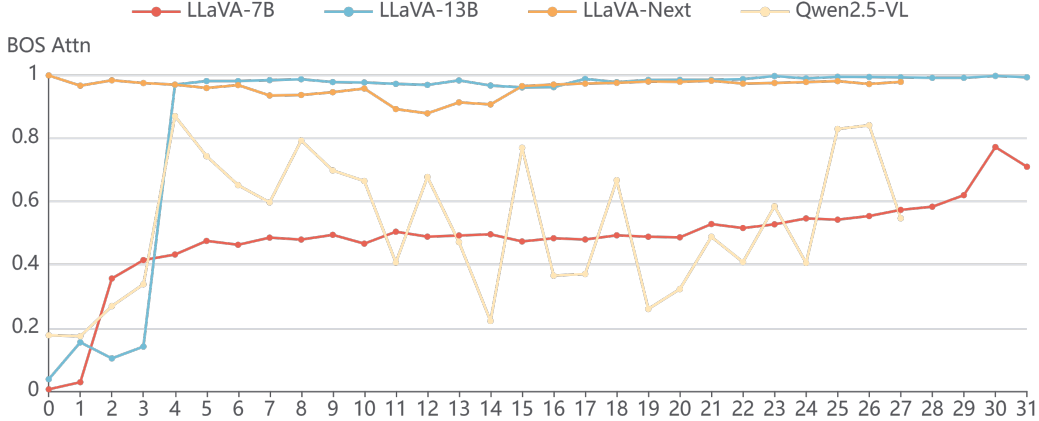


Figure 10. The model’s attention to the BOS token in each layer.

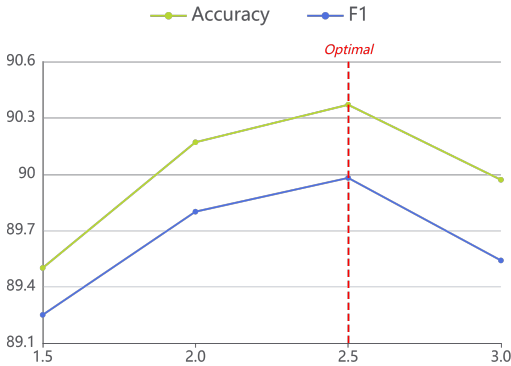


Figure 11. Effectiveness of β in MSCOCO’s Random set

is discussed in Section C. Specifically, the starting layers are set as follows (with layers numbered from 0): layer 2 for LLaVA-1.5, layer 0 for LLaVA-Next, and layer 4 for Qwen2.5-VL. We apply VGA up to an intermediate layer of the model: specifically, layer 24 for LLaVA-1.5-13B and layer 16 for all other models. We adopt the default settings of $\beta = 0.2$ and $\lambda = 0.02$. For the larger model (LLaVA-1.5-13B) and visually simpler tasks (POPE), we increase β to 0.25 to apply stronger vision guidance. Stanza [21] is utilized to extract objects mentioned in the question. We employ greedy decoding for next token prediction and set the maximum generation length to 512. All experiments are conducted using a single NVIDIA A800-40G GPU.

B. Discussion of Main Results

POPE. The experimental results on the POPE benchmark are summarized in Table 1. Our proposed method, VGA, achieves significant improvements, clearly demonstrating its advantage in mitigating existence hallucinations. Moreover, VGA consistently delivers positive gains across all tested MLLMs, highlighting its strong generalizabil-

ity. While the baselines enhance visual understanding by strengthening the model’s attention to visual content, they often lack precise localization of key objects, which leads to suboptimal performance. The superior performance of VGA indicates that providing explicit visual guidance effectively enhances the model’s ability to perceive and discriminate objects within the image.

CHAIR. The experimental results on the CHAIR benchmark are presented in Table 2. Our method achieves the overall lowest hallucination rate across all evaluated MLLMs, while maintaining no significant drop in F1 score. This result underscores VGA’s ability to strike a better balance between generating a richer output and ensuring generation accuracy. Although PAI enhanced by contrastive decoding (PAI_{CD}) further refines visual information in the logits and achieves strong performance, contrastive decoding requires two forward passes, which effectively doubles the inference cost. In stark contrast, VGA achieves superior performance with only a single forward pass, demonstrating both higher efficiency and effectiveness.

AMBER. AMBER is a comprehensive hallucination benchmark that enables a more thorough evaluation of model hallucinations. The results, shown in Table 3 and Table 5, demonstrate that VGA still achieves significant dehallucination performance, further validating the importance of precise visual guidance. Methods like TARAC guide visual attention based on historical attention distributions; however, the localization capability derived solely from visual attention is inherently limited. In contrast, VGA leverages VSC to achieve more accurate visual grounding without relying on external tools, thus enabling a more effective suppression of hallucinations.

Table 5. Results on AMBER with LLaVA-13B. The AMBER metric is calculated as $(1 - \text{CHAIR} + \text{F1})/2$.

MLLM	Method	CHAIR ↓	Cover ↑	Hal ↓	Cog ↓	Acc. ↑	Prec. ↑	Rec. ↑	F1 ↑	AMBER ↑
LLaVA-13B	Vanilla	6.8	51.3	31.1	3.4	71.5	96.0	59.5	73.5	33.85
	PAI	5.4	<u>51.6</u>	<u>27.3</u>	2.1	74.2	<u>95.6</u>	64.0	76.7	36.15
	PAI _{CD}	<u>5.2</u>	52.0	28.3	1.9	<u>75.0</u>	95.3	<u>65.5</u>	<u>77.6</u>	<u>36.70</u>
	VAF	6.9	51.2	32.0	3.6	69.5	<u>95.6</u>	56.7	71.2	32.65
	TARAC	5.8	49.3	28.5	2.9	73.0	96.0	61.9	75.3	35.25
	VGA	4.6	49.9	23.6	<u>2.0</u>	78.5	95.0	71.3	81.5	38.95

Table 6. Ablation study on CHAIR.

Setting	Cs	Ci	F1
VGA	29.8	8.2	76.3
w/o Head Balancing	34.6	9.4	76.3
w/o Early Termination	32.6	8.8	75.4

C. The Starting Layer of VGA

In self-attention mechanisms, a “sink” phenomenon [10, 36] exists—where the model abnormally focuses its attention on a few individual tokens. PAI [18] observes that the BOS token carries very limited information yet consistently receives disproportionately high attention. Consequently, when the BOS token receives excessively high attention from the model, it serves as an appropriate trigger to enhance the model’s visual attention. Following the approach of PAI, we analyze the BOS attention patterns across different models to determine the optimal starting layer for VGA. We apply max pooling across all attention heads. The analysis results on the image captioning task are shown in Figure 10. Based on our observations, we set the starting layer of VGA for different MLLMs as follows: layer 2 for LLaVA-1.5-7B, layer 4 for LLaVA-1.5-13B, layer 0 for LLaVA-Next, and layer 4 for Qwen2.5-VL.

D. Ablation Study

Considering the functional diversity across attention heads, VGA employs head balancing by applying stronger guidance to heads with weaker visual features and lighter guidance to those that already exhibit strong visual functionality. Additionally, since visual understanding in MLLMs primarily occurs in the early to middle layers, we terminate visual attention guidance at an intermediate layer of the model. We conduct ablation studies on both of these design choices, and the results are presented in Table 6. Head balancing preserves the model’s original visual capabilities while incorporating additional vision-guidance, thereby achieving improved performance. Meanwhile, the early exit mechanism prevents visual guidance from being applied during non-

Table 7. Effectiveness of β and λ in CHAIR’s validation set.

Setting	Cs	F1
Vanilla	49.6	76.5
$\beta = 0.15, \lambda = 0.01$	41.6	77.5
$\beta = 0.15, \lambda = 0.02$	43.4	76.8
$\beta = 0.15, \lambda = 0.04$	43.6	77.1
$\beta = 0.20, \lambda = 0.01$	26.2	76.4
$\beta = 0.20, \lambda = 0.02$	32.8	77.7
$\beta = 0.20, \lambda = 0.04$	38.6	77.9
$\beta = 0.25, \lambda = 0.01$	10.0	68.7
$\beta = 0.25, \lambda = 0.02$	11.8	69.1
$\beta = 0.25, \lambda = 0.04$	19.8	71.8

visual understanding stages, maintaining consistency with the model’s inherent behavioral characteristics. In short, both the head balancing and early termination modules contribute positively to performance.

E. Hyperparameters

β controls the strength of visual guidance, while λ controls the penalty strength on already-generated content in image captioning tasks. We perform a grid search for β on the POPE benchmark, as shown in Figure 11. Additionally, we conduct a grid search over both β and λ on the CHAIR benchmark, with results presented in Table 7. We observe that for tasks like POPE, which require focusing on a single visual region, stronger visual guidance is beneficial. In contrast, for image captioning tasks that demand broader attention across multiple visual regions, overly strong guidance can restrict the model’s capacity. Therefore, we set $\beta = 0.25$ on the POPE benchmark and $\beta = 0.2$ on other benchmarks. Furthermore, for image captioning, we select $\lambda = 0.02$ based on a balanced consideration of hallucination rate and F1 score.

F. Beyond Object Hallucination.

The model’s comprehension of auxiliary information, such as relations and attributes, fundamentally relies on its under-

Table 8. *Att.* and *Rel.* denote the F1 scores on AMBER’s attribute and relation tasks, respectively. *MME* denote perception tasks in the MME benchmark.

MLLM	Method	Att.	Rel.	MME
LLaVA-1.5-7B	Vanilla	64.4	68.5	1456.5
	TARAC	63.5	68.4	1462.1
	VGA	65.7	73.9	1465.7
Qwen2.5-VL-7B	Vanilla	84.4	75.8	1691.1
	TARAC	84.8	76.2	1713.1
	VGA	86.4	76.3	1719.7

standing of objects; thus, object grounding remains critical. Furthermore, for tasks lacking explicit objects (*e.g.*, image captioning), we employ the VSS mechanism to establish informative grounding (see Sec. 3.2). Additional results presented in Table 8 indicate that VGA maintains advantages in mitigating relation- and attribute-based hallucinations. We further validate VGA on general VQA benchmarks. Results on MME [5] demonstrate that VGA performs effectively on object-agnostic tasks, confirming that these performance gains stem from enhanced visual perception via vision guidance.

G. First Token Approximation.

We approximate the visual semantic confidence of an object using the first token of its tokenized representation. Under a single-step prediction setting, utilizing the first token aligns with the autoregressive paradigm; conversely, the probability of any non-first token (without the “_” prefix) is extremely low (always less than $1e - 4$), rendering their distribution across visual tokens meaningless. We also experimented with aggregating the probabilities of all tokens ($\log c(O) \approx \sum_i \log c(o_i)$); however, this yielded negligible performance differences. Consequently, we adopt the simplest approach.